

Direct numerical simulations of compressible isothermal turbulence in a periodic box: Reynolds number and resolution-level dependence

Yoshiki Sakurai*

Faculty of Environment and Information Sciences, Yokohama National University, Yokohama 240-8501, Japan

Takashi Ishihara[†]Faculty of Environmental, Life, Natural Science and Technology, Okayama University,
Okayama 700-8530, Japan

(Received 19 January 2023; accepted 3 August 2023; published 28 August 2023)

A series of direct numerical simulations (DNSs) of forced compressible isothermal turbulence in a periodic box are conducted by using an eighth-order compact finite-difference scheme to study the Reynolds number and resolution-level ($k_{\max}\eta$) dependence of the statistics of the compressible turbulence, where $k_{\max} = \sqrt{3}N/2$, η the Kolmogorov length scale. The number of grid points N^3 and the Taylor microscale Reynolds number R_λ are up to 4096^3 and 853, respectively, and the turbulent Mach number and the ratio of dilatational to solenoidal root-mean-square velocities are approximately 0.3 and 0.4, respectively. The DNSs have shown that the energy spectrum for the compressible isothermal turbulence increases to a higher wave-number range of $k\eta > 1$ with increasing resolution levels suggesting a k^{-3} scaling of its dilatational component; however, the energy spectrum and its solenoidal and dilatational components for $k\eta < 1$ are not sensitive to resolution levels provided that $k_{\max}\eta \gtrsim 2$. When the solenoidal quantities are used for normalization, the solenoidal component of the energy spectrum and the solenoidal dissipation rate agree well with those gathered from the DNSs of incompressible turbulence. DNS studies indicate that the normalized dilatational component of energy dissipation is still finite nonzero for large R_λ values (as opposed to an expectation from the result by John *et al.* [*J. Fluid Mech.* **920**, A20 (2021)]). The PDFs of the solenoidal component of pressure fluctuations agree with those of incompressible turbulence. However, a close study shows that the solenoidal pressure and enstrophy fluctuations in compressible isothermal turbulence are consistently less intermittent than those in incompressible turbulence. The impact of bulk viscosity on the energy spectrum is examined using the DNSs of compressible isothermal turbulence with nonzero bulk viscosity.

DOI: [10.1103/PhysRevFluids.8.084606](https://doi.org/10.1103/PhysRevFluids.8.084606)

I. INTRODUCTION

Turbulence is fundamentally essential in science and engineering. We may roughly classify many of the turbulent flows around us as incompressible ones. Theoretically, incompressible turbulence may be easier to study than compressible turbulence, because it lacks any parameters that determine the flow's compressibility. Therefore, flows are often assumed as incompressible in turbulence studies. However, turbulent airflows are weakly compressible depending on the circumstances. Additionally, compressibility plays a significant role in many turbulent flows in astrophysics and

*sakurai-yoshiki-hx@ynu.ac.jp

†takashi_ishihara@okayama-u.ac.jp

mechanical engineering. Therefore, deepening our understanding of both incompressible and compressible turbulent flows, and the relationship between them, is desired in science and engineering.

Direct numerical simulation (DNS) of turbulence is a powerful tool for studying the characteristics of turbulence. With the development of supercomputers, this tool has become strongly advanced. Regarding incompressible turbulence, the Fourier spectral method has been widely applied to DNSs of homogeneous isotropic turbulence in a periodic box. The DNS data enable us to carefully evaluate the universality of the statistics of the small-scale turbulent motions in detail [1]. As anticipated by Kolmogorov's theory, DNS studies of incompressible turbulence at high Reynolds numbers have confirmed that the finiteness of the normalized mean-energy dissipation rate per unit mass and the presence of inertial subrange in the energy spectrum. Recent large-scale DNSs of turbulence with the number of grid points and the Taylor microscale Reynolds number R_λ up to $12\,288^3$ and approximately 2300, respectively, showed that the wave-number (k) range of the energy spectrum could be separated into three categories, including F (flat), T (tilted), and B (bump) ranges [2]: The compensated energy spectrum, $E(k)/(\epsilon^{2/3}k^{-5/3})$, is almost flat in the F range, moderately tilted in the T range, and has a bump in the high wave-number range (B range), where ϵ is the mean rate of energy dissipation per unit mass. The existence of the spectral bump in the B range has also been known in a numerical study based on the vortex blob method [3]. The T range in the energy spectrum can be observed in Refs. [1,4,5]. It has been shown in Ref. [2] that the energy spectrum fits well to a power law in the T range, but the pre-factor depends on R_λ . This result implies that the statistics in the T range are not necessarily free from the viscosity. Regarding the F range, DNSs with larger R_λ and longer simulation times are awaited to examine R_λ dependence. However, the larger-scale DNS based on the Fourier spectral method has become more challenging for us to perform longer on recent petascale supercomputers because data transfer occupies almost all of the computational elapsed time.

Numerical simulations of compressible turbulence based on high-order and high-resolution finite difference methods have been actively conducted to understand the effect of compressibility on turbulence (e.g., see Refs. [6–10]). These studies revealed that fluctuations in fluid density lead to the generation of shocklets (weak shock waves) even in weakly compressible turbulence. However, compared to incompressible turbulence, the maximum numbers of grid points and R_λ the DNSs of compressible box turbulence are limited to 2048^3 and 430, respectively [9,10]. In compressible turbulence, the flow velocity \mathbf{u} can be split into a solenoidal component \mathbf{u}_s and a dilatational component \mathbf{u}_d by Helmholtz decomposition [7], where $\nabla \cdot \mathbf{u}_s = 0$ and $\nabla \times \mathbf{u}_d = \mathbf{0}$. The kinetic energy spectrum of the solenoidal component is very close to that of incompressible flow and the dilatational component depends significantly on the Mach number [11]. Wang *et al.* [12] reported that the kinetic energy spectrum of \mathbf{u} exhibits $k^{-5/3}$ scaling in the inertial range, while that of \mathbf{u}_d exhibits k^{-2} scaling in that range. Donzis and Jagannathan [9] analyzed a DNS database of compressible turbulence with purely solenoidal forcing and demonstrated that the energy spectra for $R_\lambda \approx 38$ –430 and the turbulent Mach number $M_t \approx 0.1, 0.3, 0.6$ are entirely consistent with incompressible results. Numerical simulations with solenoidal forcing at M_t from 0.05 to 1.0 and at R_λ from 40 to 350 by Wang *et al.* [13] are basically consistent with those in Ref. [9]. Recently, Donzis and John [14] demonstrated that the statistics of compressible turbulence depend on the ratio $\delta \equiv u_d/u_s$, in addition to R_λ and M_t , where u_s and u_d are the root-mean-square (rms) values of the solenoidal and dilatational components of the velocity field, respectively. The value of δ varies with the ratio of the solenoidal and dilatational components of external forcing injected at a small wave-number range. Therefore, it is essential to analyze how consistent the solenoidal component of the energy spectrum in compressible turbulence produced by the forcing that has a dilatational component is with the energy spectrum in incompressible turbulence.

Donzis and John [14] studied the scaling properties in homogeneous compressible turbulence. They confirmed a relationship $\epsilon_r \equiv \epsilon_d/\epsilon_s \approx \delta^2$ by all data from different flows, different forcing schemes, and different conditions. Here ϵ_s and ϵ_d are the solenoidal and dilatational energy dissipation rates, respectively. Mach number and Reynolds number scalings of ϵ_r were proposed based on numerical simulations with solenoidal forcing by Wang *et al.* [13]. However, Donzis and John

[14] demonstrated that such scalings do not hold generally if nonsolenoidal forcing is used. John *et al.* [15] used a database of DNS throughout a broad parameter space $R_\lambda \approx 8\text{--}450$, $M_t \approx 0.05\text{--}0.8$, $\delta \approx 10^{-3}\text{--}7.0$ to study the dissipative anomaly in compressible turbulence. First, they introduced the energy dissipation rate ϵ_s and the Reynolds number R_λ^s calculated using the solenoidal component of the velocity field. They observed that the normalized values of ϵ_s asymptotically approach a finite nonzero value as R_λ^s increases. Next, the energy dissipation rate ϵ_d and Reynolds number R_λ^d were calculated using the dilatational component of the velocity field. In the parameter range studied in Ref. [15], the normalized values of ϵ_d decrease with the increase in R_λ^d , and no asymptotic approach was discovered. Therefore, large-scale DNSs of compressible turbulence with higher Reynolds numbers are required to observe the asymptotic R_λ^d dependence of ϵ_d .

DNS studies of incompressible turbulence and experimental studies show that the probability density function (PDF) of the pressure fluctuations in turbulence is negatively skewed [16–21]. The low-pressure regions are believed to be produced by the vortex tubes [22]. Using a DNS database of compressible turbulence with purely solenoidal forcing, Donzis and Jagannathan [9] demonstrated that the skewness of the PDF of pressure fluctuations changes from negative to positive as the values of M_t increase, and the transition occurs at $M_t \approx 0.3$. The fluctuating pressure can be decomposed into solenoidal and dilatational components [23]. Sakurai *et al.* [24] conducted DNSs of compressible turbulence with $R_\lambda \approx 190\text{--}440$, $M_t \approx 0\text{--}0.3$, and $\epsilon_r \approx 0\text{--}0.1$. They showed that the PDF of pressure fluctuation depends on both M_t and ϵ_r , and also that the PDFs of solenoidal pressure agree well with those of the pressure fluctuations in incompressible turbulence.

The effects of spatial resolution on small-scale statistics of turbulence in DNSs have been discussed in the past 20 years [25–33]. As shown in Jimenez *et al.* [34] by DNS of incompressible turbulence, the average radius of microscale vortices (formed by the solenoidal turbulent field) is approximately $3\eta\text{--}5\eta$, where η is the Kolmogorov length scale. However, in compressible turbulence, the dilatational component of velocity may form smaller flow structures such as shocklets. As demonstrated in Ref. [35], the most typical thickness of shocklets is a slightly decreasing function of M_t and is as tiny as 1.5η for $M_t \approx 0.9$. This shows that effective assessment of the impact of fluid compression in small-scale turbulence requires high-resolution simulation. Several studies have examined the effects of resolution on compressible turbulent fields [35–39]. Wang *et al.* [37] performed numerical simulations of compressible turbulence with various resolutions ($k'_{\max}\eta = 1.65, 2.47$, and 3.33 , where $k'_{\max} = N/2$ and N is the number of grid points in each Cartesian coordinate). They showed that, except for extremely strong compression regions, the PDFs of the normalized dilatation overlap almost everywhere. They also indicated that the observed energy spectra of the velocity field converge under the grid refinement. However, the resolution levels much higher than 3 were not performed in their study, and it has not yet been clear whether the finest structure formed by the dilatational component of the turbulent field is accurately captured. Note that the finest scale in compressible turbulence may depend on the values of the bulk viscosity appearing in the Navier-Stokes equations, which is generally assumed to be zero for dilute monatomic gases. By conducting additional DNSs with nonzero bulk viscosity, we will study its effects on the high wave-number range of the energy spectrum. See the Appendix for details.

Several numerical simulations of compressible turbulence [6–10] have been performed under nonisothermal conditions, in which the energy conservation equation is solved to determine the total energy (or the temperature). Alternatively, if we consider the compressible turbulence of isothermal fluid, then we need not solve the energy equation. In the field of astrophysics, numerical simulations of compressible isothermal turbulence are often used to study the fluid density distribution in the interstellar medium [40–44] and the clustering and dynamics of dust particles in protoplanetary disks [24,45] and molecular clouds [46–48]. Notably, in the case of very high Mach numbers, including the case of the interstellar medium, it was shown that the density variance in isothermal turbulence is different from that in nonisothermal turbulence [44]. However, Sakurai *et al.* [24] showed that when M_t is small ($M_t \lesssim 0.3$), the statistics of the motion of the inertial particles in compressible isothermal turbulence agree well with those in nonisothermal turbulence. Their results

show no remarkable differences between the statistics of isothermal and nonisothermal turbulence when M_t is small.

Here, we perform a series of the DNSs of compressible isothermal turbulence and compare the results with those of compressible nonisothermal and incompressible turbulence to discuss their similarities and differences. Additionally, we study the resolution dependence of the statistics by comparing the DNSs with different values of $k_{\max}\eta$, in which the maximum wave number k_{\max} is defined by $k_{\max} = \sqrt{2}N/3$ as used in the DNSs of incompressible turbulence [29]. Then, by using the DNSs of compressible isothermal turbulence with the grid points and the Taylor-scale Reynolds number up to $N^3 = 4096^3$ and $R_\lambda = 853$, respectively, we study the scaling properties of the energy spectra and the energy dissipation rates. The main questions addressed in this paper are the following.

(1) How do the solenoidal and dilatational energy dissipation rates behave when the Reynolds number is high?

(2) How does the spatial resolution of the DNS of compressible turbulence affect such statistics as the energy spectrum?

(3) Does the solenoidal component of the energy spectrum in the inertial subrange of weakly compressible isothermal turbulence conform to that of incompressible turbulence?

In Sec. II, we briefly describe a series of our DNSs of compressible isothermal turbulence. In Sec. III, we present our results by comparing those in compressible nonisothermal and incompressible turbulence and discuss the resolution and Reynolds number dependence of turbulent statistics. In Sec. IV, we summarize our results as conclusions. Finally, in the Appendix, the effect of the bulk viscosity on the energy spectra of compressible isothermal turbulence is discussed on the basis of DNSs of compressible isothermal turbulence with nonzero bulk viscosity.

II. METHODS OF DIRECT NUMERICAL SIMULATIONS

A. Governing equations

This study considers the three-dimensional homogeneous isotropic turbulence of compressible fluid. The compressible fluid is assumed to be isothermal and to be governed by the following equations:

$$\frac{\partial \rho}{\partial t} + \frac{\partial \rho u_j}{\partial x_j} = 0, \quad (1)$$

$$\frac{\partial \rho u_i}{\partial t} + \frac{\partial (\rho u_i u_j + p \delta_{ij})}{\partial x_j} = \frac{\partial \tau_{ij}}{\partial x_j} + f_i, \quad (2)$$

$$p = \rho c^2, \quad (3)$$

where ρ is the density, u_i and f_i are the i th components of the velocity and external force, p is the pressure, and c is the speed of sound. The viscous stress tensor τ_{ij} is given by

$$\tau_{ij} = \mu \left(\frac{\partial u_i}{\partial x_j} + \frac{\partial u_j}{\partial x_i} - \frac{2}{3} \theta \delta_{ij} \right), \quad (4)$$

where $\theta \equiv \partial u_k / \partial x_k$ is the velocity divergence, and the dynamic viscosity μ is constant in the isothermal turbulence. Note that μ may depend on the temperature in the nonisothermal turbulence.

The forcing f_i in Eq. (2) is added to maintain a statistically quasistationary state of turbulence. We use the forcing scheme proposed by Ref. [49], which can adjust the ratio of the dilatational to solenoidal component of the turbulent field. The Fourier coefficient of f_i is not zero only at low wave numbers $|k| < 3$, and f_i is given by

$$f_i = c_s \sqrt{\rho} \bar{w}_{i_s} + c_d \sqrt{\rho} \bar{w}_{i_d}, \quad (5)$$

where \bar{w}_{i_s} and \bar{w}_{i_d} are the solenoidal and dilatational components of the spectrally filtered density-weighted velocity obtained by setting the Fourier coefficient of $w_i \equiv \sqrt{\rho} u_i$ for $|k| \geq 3$ to zero,

respectively, the two coefficients are determined by

$$c_s = \frac{\epsilon_s \text{ target}}{\langle \bar{w}_i w_i \rangle} \quad \text{and} \quad c_d = \frac{\epsilon_d \text{ target} - \langle \theta p \rangle}{\langle \bar{w}_{id} w_i \rangle},$$

where we specify the values of $\epsilon_{\text{target}} = \epsilon_s \text{ target} + \epsilon_d \text{ target}$ and $\epsilon_r \text{ target} = \epsilon_d \text{ target} / \epsilon_s \text{ target}$ to keep the energy dissipation per unit mass $\epsilon = \langle \tau_{ij} (\partial u_i / \partial x_j) \rangle / \langle \rho \rangle$ and $\epsilon_r = \epsilon_d / \epsilon_s$ approximately constant. Here, the solenoidal and dilatational dissipation per unit mass is defined as $\epsilon_s = \nu \langle |\boldsymbol{\omega}|^2 \rangle$ and $\epsilon_d = (4/3)\nu \langle \theta^2 \rangle$, respectively, where $\nu = \langle \mu \rangle / \langle \rho \rangle$ [50] and $\boldsymbol{\omega} = \nabla \times \mathbf{u}$. The values of $\epsilon_r \text{ target}$ were set to 0.1 for all runs of compressible isothermal turbulence, and the values of ϵ_{target} were set to those of $\langle \epsilon \rangle$ obtained by the DNSs with the same grid points in Table 1 of Ref. [29]. Readers refer to Ref. [49] for the details of the forcing scheme.

In this paper, we compare the results of the DNSs of compressible isothermal turbulence with those of compressible nonisothermal turbulence in Ref. [24] and those of incompressible turbulence in Refs. [29,51]. Here, we briefly review the governing equations used in the DNSs of the compressible nonisothermal and incompressible turbulence for the readers' convenience.

In the DNS of compressible nonisothermal turbulence [24], Eqs. (1) and (2), and the total energy equation

$$\frac{\partial \rho E}{\partial t} + \frac{\partial (\rho E u_j + p u_j)}{\partial x_j} = \frac{\partial (\tau_{ij} u_i - q_j)}{\partial x_j} + f_j u_j + f_e \quad (6)$$

are used. Here τ_{ij} is given by Eq. (4), and the total energy E and heat flux q_i are given by

$$E = \frac{1}{2} u_j u_j + e \quad \text{and} \quad q_i = -\kappa \frac{\partial T}{\partial x_i},$$

respectively, where e is the internal energy, κ is the thermal conductivity, and T is the temperature. The dynamic viscosity and thermal conductivity are assumed to be given by $\mu = \mu_0 (T/T_0)^{0.76}$ and $\kappa = \kappa_0 (T/T_0)^{0.76}$, where μ_0 and κ_0 are the reference (dimensional) constants and T_0 is the reference temperature [7]. The cooling function f_e in Eq. (6) is set to be $f_e = -f_j u_j$ to conserve the total energy as in Ref. [49]. The equation of state of an ideal gas

$$p = \rho RT \quad (7)$$

is used to close the set of equations, where R is the gas constant of the fluid, the sound speed is given by $c = \sqrt{\gamma RT}$, and $\gamma = C_p / C_v$ is the ratio of the specific heat at constant pressure C_p to that at constant volume C_v . The Prandtl number $Pr \equiv \mu_0 C_p / \kappa_0 = 0.7$ and the ratio of specific heat $\gamma = 1.4$ are used.

In the DNS of incompressible turbulence of unit density ($\rho = 1$) [29,51], the Navier-Stokes equation

$$\frac{\partial u_i}{\partial t} + \frac{\partial (u_i u_j + p \delta_{ij})}{\partial x_j} = \frac{\partial \tau_{ij}}{\partial x_j} + f_i^I \quad (8)$$

and the continuity equation

$$\frac{\partial u_j}{\partial x_j} = 0 \quad (9)$$

are used, where $\tau_{ij} = \nu (\partial u_i / \partial x_j + \partial u_j / \partial x_i)$, the kinematic viscosity ν is constant, and f_i^I is the incompressible forcing (e.g., see Ref. [29] for the details of f_i^I).

B. Numerical method and running conditions

The turbulence field is assumed to be periodic in each direction of the Cartesian coordinates with a fundamental periodic box of size 2π . In the DNS of compressible isothermal turbulence, the eighth-order compact difference (CD) scheme [52] and the eighth-order central finite difference

TABLE I. Simulation parameters and turbulence characteristics. C256-1-nonIT, C512-1-nonIT, C1024-1-nonIT, I256-1, I512-1, and I1024-1 are from Ref. [24] (note that M_{rms} in Ref. [24] is equivalent to M_t in this paper). I512-2 and I1024-2 are from Ref. [29]. I2048-2 and I4096-2 are from Ref. [51].

Run	N^3	$k_{\text{max}}\eta$	$10^3\Delta t$	10^{-3}Re	R_λ	M_t	δ	ϵ_r	$10^2\epsilon$	L	λ	$10^3\eta$	u
C256-1	256 ³	1.00	1.0	1.00	185	0.31	0.39	0.097	7.64	1.19	0.219	8.19	0.590
C512-1	512 ³	1.03	0.5	2.93	354	0.30	0.39	0.101	6.97	1.29	0.156	4.21	0.635
C1024-1	1024 ³	1.02	0.5	6.75	514	0.32	0.40	0.077	7.01	1.22	0.0931	2.09	0.607
C2048-1	2048 ³	1.04	0.1	17.4	853	0.32	0.40	0.071	6.61	1.25	0.0612	1.07	0.613
C512-2	512 ³	1.99	0.5	1.08	183	0.31	0.39	0.110	7.84	1.28	0.217	8.14	0.592
C1024-2	1024 ³	1.99	0.5	2.84	326	0.33	0.39	0.098	8.02	1.26	0.145	4.07	0.632
C2048-2	2048 ³	2.01	0.1	7.09	520	0.32	0.40	0.094	7.46	1.26	0.0923	2.06	0.620
C4096-2	4096 ³	2.06	0.1	17.2	840	0.32	0.41	0.092	6.96	1.23	0.0600	1.05	0.616
C2048-4	2048 ³	4.05	0.1	2.89	337	0.33	0.40	0.120	7.48	1.28	0.150	4.14	0.631
C4096-8	4096 ³	8.08	0.1	2.89	336	0.33	0.40	0.126	7.55	1.28	0.149	4.13	0.631
C256-1-nonIT	256 ³	1.01	1.0	1.11	193	0.32	0.36	0.089	7.34	1.27	0.220	8.28	0.614
C512-1-nonIT	512 ³	1.03	0.5	2.78	316	0.32	0.38	0.080	7.12	1.26	0.144	4.20	0.618
C1024-1-nonIT	1024 ³	1.05	0.5	5.69	437	0.30	0.38	0.061	6.44	1.11	0.0863	2.14	0.560
I256-1	256 ³	0.96	1.0	0.933	167	—	—	—	8.50	1.13	0.203	7.97	0.577
I512-1	512 ³	0.98	0.5	2.26	286	—	—	—	7.89	1.09	0.139	4.08	0.577
I1024-1	1024 ³	1.00	0.5	6.43	458	—	—	—	7.22	1.22	0.0873	2.07	0.577
I512-2	512 ³	1.96	1.0	1.00	173	—	—	—	7.95	1.21	0.210	8.10	0.577
I1024-2	1024 ³	1.95	0.625	2.31	268	—	—	—	8.29	1.12	0.130	4.03	0.577
I2048-2	2048 ³	1.97	0.4	5.84	446	—	—	—	7.62	1.11	0.0849	2.04	0.577
I4096-2	4096 ³	2.02	0.25	14.8	730	—	—	—	7.11	1.13	0.0556	1.05	0.577

scheme are used to calculate the advection and the viscous terms, respectively, as in the case of compressible nonisothermal turbulence [24]. The CD scheme was implemented by solving tridiagonal matrix problems in parallel with the method developed by Mattor *et al.* [53]. The time marching is conducted using the third-order TVD Runge-Kutta method [54] with a constant time step (Δt). The eighth-order low-pass filter [55] removes nonphysical numerical oscillations that may occur in the high-frequency region. For incompressible turbulence, Eqs. (8) and (9) are solved numerically by a fully alias-free spectral method, where aliasing errors are removed using the so-called phase-shift method, which keeps all the Fourier modes satisfying $k < k_{\text{max}} = \sqrt{2}N/3$. The time marching is performed by a fourth-order Runge-Kutta method. See Ref. [29] for details of the methods for DNS of incompressible turbulence.

The simulation parameters and turbulence characteristics in the DNSs are summarized in Table I. The run names for compressible turbulence consist of the initial character ‘‘C’’ representing a compressible flow, the number of grid points (N) in each Cartesian coordinate, and the integer, which represents the resolution level defined as the approximate value of $k_{\text{max}}\eta (\approx 3\eta/\Delta x$, where $\Delta x = 2\pi/N$). The character ‘‘nonIT’’ follows the resolution level for compressible nonisothermal turbulence. The run names for incompressible turbulence consist of the initial character ‘‘I’’ representing an incompressible flow, N , and the integer representing the resolution level ($k_{\text{max}}\eta$ with $k_{\text{max}} = \sqrt{2}N/3$).

The statistics for runs with $N^3 = 256^3$, 512^3 , and 1024^3 were obtained through time averaging (except for I512-2 and I1024-2). As demonstrated in Refs. [14,24], the properties of compressible turbulence depend on the values M_t and δ (or $\epsilon_r \approx \delta^2$). In our DNSs and a part of those in Ref. [24], target values of M_t and ϵ_r are set to 0.3 and 0.1, respectively, and their resulting values are also

shown in Table I. The energy dissipation per unit mass, $\epsilon = \langle \tau_{ij}(\partial u_i/\partial x_j) \rangle / \langle \rho \rangle$, is computed by

$$\epsilon = \nu \left(\langle |\boldsymbol{\omega}|^2 \rangle + \frac{4}{3} \langle \theta^2 \rangle \right), \quad (10)$$

where $\nu = \mu/\langle \rho \rangle$ in compressible isothermal turbulence whereas ν is a given constant and $\langle \theta^2 \rangle = 0$ in incompressible turbulence. We set $\langle \rho \rangle = 1$ in the DNSs in Table I. Note that, in general,

$$2 \int_0^\infty k^2 E(k) dk = \langle |\boldsymbol{\omega}|^2 \rangle + \langle \theta^2 \rangle, \quad (11)$$

where $E(k)$ is the three-dimensional energy spectrum. The integral length scale L and the Kolmogorov length scale η are, respectively, calculated as

$$L = \frac{\pi}{2u^2} \int_0^\infty k^{-1} E(k) dk \quad (12)$$

and $\eta = (\nu^3/\epsilon)^{1/4}$ in both compressible and incompressible turbulence. Here, u is the rms value of the fluctuating velocity in one direction and is related to $E(k)$ as

$$\frac{3}{2} u^2 = \int_0^\infty E(k) dk. \quad (13)$$

The Taylor microscale is computed by $\lambda = (15\nu u^2/\epsilon)^{1/2}$. The Reynolds number Re and the Taylor microscale Reynolds number R_λ are calculated as $\text{Re} = uL/\nu$ and $R_\lambda = u\lambda/\nu$, respectively. The turbulent Mach number M_t is calculated by $M_t = \sqrt{\langle 3u^2 \rangle} / \langle c \rangle$.

We decompose turbulence characteristics into their solenoidal and dilatational components to assess the scaling for the solenoidal and dilatational parts separately. The energy dissipation rate may be decomposed into $\epsilon = \epsilon_s + \epsilon_d$, each of which is calculated as

$$\epsilon_s = \nu \langle |\boldsymbol{\omega}|^2 \rangle = 2\nu \int_0^\infty k^2 E_s(k) dk, \quad (14)$$

$$\epsilon_d = (4/3)\nu \langle \theta^2 \rangle = (8/3)\nu \int_0^\infty k^2 E_d(k) dk, \quad (15)$$

respectively [50]. Here $E_s(k)$ and $E_d(k)$ are the solenoidal and dilatational components of the energy spectrum. Following Ref. [15], we calculate the decomposed Taylor Reynolds number and decomposed integral length scale as

$$R_\lambda^s = R_\lambda \left(\frac{u_s}{u} \right)^2 \sqrt{\frac{\epsilon}{\epsilon_s}}, \quad R_\lambda^d = R_\lambda \left(\frac{u_d}{u} \right)^2 \sqrt{\frac{\epsilon}{\epsilon_d}}, \quad (16)$$

$$L_s = \frac{\pi}{2u_s^2} \int_0^\infty k^{-1} E_s(k) dk, \quad L_d = \frac{\pi}{2u_d^2} \int_0^\infty k^{-1} E_d(k) dk, \quad (17)$$

respectively. The decomposed solenoidal and dilatational values of R_λ , ϵ , L , and u are summarized in Table II.

III. NUMERICAL RESULTS

A. Energy dissipation rate

A basic assumption of turbulence theories, including Kolmogorov (1941) [56], is that the dissipation rate remains finite as the viscosity tends to zero. This fundamental turbulence principle is commonly known as ‘‘dissipative anomaly’’ and is also called the ‘‘zeroth law of turbulence.’’ Therefore, Reynolds number dependence of the normalized average energy dissipation rate,

$$D \equiv \frac{\epsilon L}{u^3}, \quad (18)$$

TABLE II. Solenoidal and dilatational components of turbulence characteristics for compressible turbulence. $D = \epsilon L/u^3$, $D_s = \epsilon_s L_s/u_s^3$, and $D_d = \epsilon_d L_d/u_d^3$. C256-1-nonIT, C512-1-nonIT, and C1024-1-nonIT are from Ref. [24].

Run	R_λ	R_λ^s	R_λ^d	$10^2 \epsilon$	$10^2 \epsilon_s$	$10^2 \epsilon_d$	L	L_s	L_d	u	u_s	u_d	D	D_s	D_d
C256-1	185	168	80.9	7.64	6.97	0.673	1.19	1.14	1.52	0.590	0.551	0.213	0.440	0.474	1.06
C512-1	354	322	153	6.97	6.34	0.638	1.29	1.25	1.58	0.635	0.592	0.230	0.352	0.381	0.830
C1024-1	514	460	265	7.01	6.51	0.502	1.22	1.17	1.57	0.607	0.564	0.225	0.383	0.424	0.688
C2048-1	853	761	453	6.61	6.17	0.441	1.25	1.20	1.57	0.613	0.569	0.227	0.358	0.400	0.594
C512-2	183	168	75.7	7.84	7.06	0.777	1.28	1.24	1.53	0.592	0.552	0.213	0.483	0.521	1.22
C1024-2	326	298	141	8.02	7.31	0.714	1.26	1.21	1.57	0.632	0.589	0.227	0.401	0.433	0.962
C2048-2	520	470	241	7.46	6.82	0.639	1.26	1.20	1.59	0.620	0.577	0.229	0.393	0.428	0.853
C4096-2	840	749	422	6.96	6.37	0.584	1.23	1.17	1.59	0.616	0.569	0.235	0.366	0.403	0.715
C2048-4	337	308	141	7.48	6.68	0.801	1.28	1.23	1.59	0.631	0.586	0.233	0.382	0.409	1.00
C4096-8	336	307	137	7.55	6.71	0.842	1.28	1.23	1.58	0.631	0.587	0.233	0.384	0.410	1.05
C256-1-nonIT	193	179	76.2	7.34	6.72	0.597	1.27	1.23	1.59	0.614	0.578	0.206	0.403	0.427	1.09
C512-1-nonIT	316	287	149	7.12	6.57	0.529	1.26	1.20	1.66	0.618	0.577	0.221	0.379	0.409	0.821
C1024-1-nonIT	437	393	228	6.44	6.07	0.376	1.11	1.06	1.47	0.560	0.523	0.199	0.407	0.447	0.705

has been extensively examined in turbulence studies, e.g., experiments by Refs. [57–59] and numerical simulations by Refs. [60–65]. An analytical upper bound for dissipation is given by Doering and Foias [66] for incompressible turbulence, and Donzis *et al.* [63] used their analytical expression to fit incompressible data of D . An extensive discussion of a dissipative anomaly in incompressible turbulence can be found in Ref. [67].

Figure 1(a) compares the values of D obtained from the compressible data in Table I with those for incompressible turbulence plotted in Ref. [62]. The results show that both D values remain finite as R_λ becomes large and that D 's values for compressible turbulence are slightly smaller than those for incompressible turbulence. Figure 1(b) demonstrates that the present values of D agree well with the compressible results plotted in Ref. [15]. This agreement confirms that the classical incompressible scaling does not hold for the total dissipation field [15]. The value of D in Eq. (18) can be considered a ratio of the average energy dissipation rate to the value of u^3/L , where the later is in the order of the average energy input rate on a large scale. Therefore, the results in Fig. 1 imply that the ratio in high Re compressible turbulence may be slightly smaller than that in high

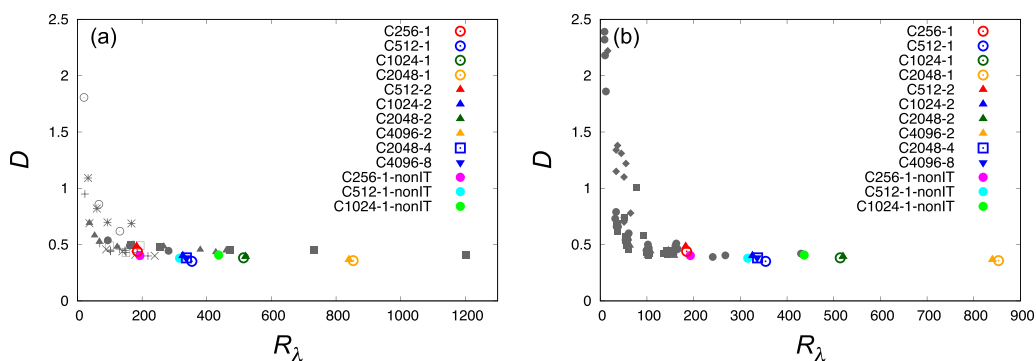


FIG. 1. (a) Comparison of the values of normalized energy dissipation, $D \equiv \epsilon L/u^3$, obtained from the DNSs of compressible turbulence with those of incompressible turbulence (from Ref. [62]), plotted as a function of R_λ and (b) the same plot compared with those from compressible simulations in Ref. [15].

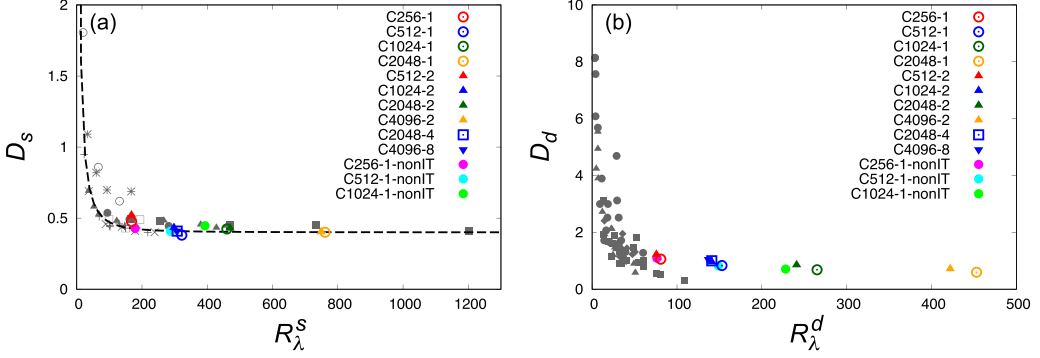


FIG. 2. (a) Solenoidal dissipation normalized by solenoidal variables, $D_s \equiv \epsilon_s L_s / u_s^3$, as a function of R_λ^s and (b) dilatational dissipation normalized by dilatational variables, $D_d \equiv \epsilon_d L_d / u_d^3$, as a function of R_λ^d . The dashed line in (a) corresponds to the function $D_s = (C_\infty^s/2)(1 + \sqrt{1 + (R_{\lambda,cr}^s/R_\lambda^s)^2})$ with $C_\infty^s = 0.4$ and $R_{\lambda,cr}^s = 92$. The values of C_∞^s and $R_{\lambda,cr}^s$ are obtained for incompressible flows in Ref. [68]. The data from Refs. [62] and [15] are plotted as gray points in panels (a) and (b), respectively.

Re incompressible turbulence. However, we should note that the solenoidally forced cases follow a trend similar to that for incompressible turbulence, as reported in Jagannathan and Donzis [10].

According to John *et al.* [15], the relationship between normalized energy dissipation rate and Reynolds number in compressible turbulence can be assessed using the solenoidal and dilatational components of the energy dissipation rate separately. In Fig. 2(a), we plot solenoidal dissipation normalized by solenoidal variables, $D_s \equiv \epsilon_s L_s / u_s^3$, as a function of the solenoidal Taylor Reynolds number R_λ^s . The normalized solenoidal energy dissipation rate values keep a constant value (≈ 0.4) in the $R_\lambda^s \approx 168$ –761 and conform to the incompressible results. These high Reynolds number results support that the characteristics of the solenoidal energy dissipation rate in compressible turbulence are virtually the same as those of the energy dissipation rate in incompressible turbulence.

To investigate the asymptotic behavior of the normalized dilatational dissipation rate, $D_d \equiv \epsilon_d L_d / u_d^3$, in compressible turbulence, we examine the R_λ^d dependence obtained in both compressible isothermal turbulence and compressible nonisothermal turbulence. John *et al.* [15] mentioned that if asymptotic scaling of the dilatational dissipation rate exists, the asymptotic value is zero. However, the R_λ^d values in their DNS seem not to be high enough. The range of the dilatational component of R_λ in our DNSs is $R_\lambda^d = 75.7$ –453, which means that R_λ^d dependence of ϵ_d can be investigated in a higher R_λ^d range than John *et al.* [15]. Since the values related to the compressibility of turbulence are set as $M_t \approx 0.3$ and $\delta \approx 0.4$ (or $\epsilon_r \approx 0.1$) in this study (see Table I), the dilatational components of the integral length scale L_d and the rms value of the velocity u_d are almost the same values for different runs (see Table II). However, the values of ϵ_d , which are related to the viscosity rate μ , are a decreasing function of the Reynolds number. This observation indicates that the D_d values tend to be zero at high R_λ^d as described in John *et al.* [15]. Figure 2(b) shows that D_d is a slightly decreasing function of R_λ^d ; however, the value is approximately 0.5 at $R_\lambda^d \approx 400$. This result shows (i) the dilatational dissipation rate may remain finite nonzero in the limit $R_\lambda^d \rightarrow \infty$ like the solenoidal component, or (ii) it may approach to zero, but the approach is slow. The DNSs of compressible turbulence under various conditions with even higher Reynolds numbers should be conducted to confirm these conjectures.

As for the values of D , D_s , and D_d in the DNSs of compressible turbulence, their dependence on the resolution level defined by the value of $k_{\max} \eta (\approx 3\eta / \Delta x)$ has not been so remarkable. However, careful observation reveals a small but finite systematic dependence. For example, the values of R_λ , M_t , and δ in Runs C256-1, C512-1, C1024-1, and C2048-1 (resolution level 1) are approximately similar to those in Runs C512-2, C1024-2, C2048-2, and C4096-2 (resolution level 2), respectively.

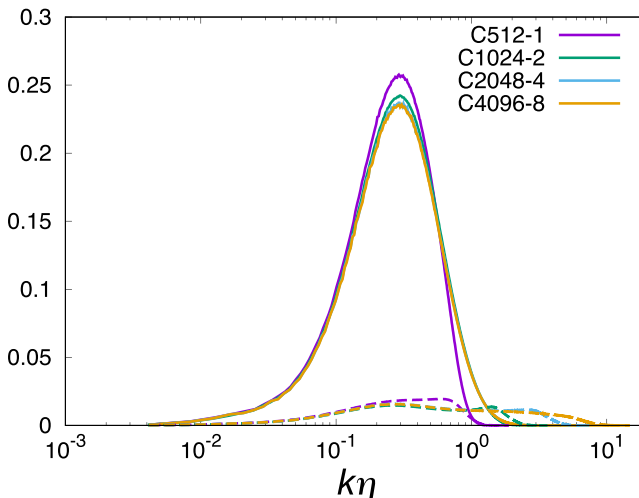


FIG. 3. Linear-log plots of $(k\eta)^3 E_s(k)/(\epsilon v^5)^{1/4}$ (solid lines) and $(4/3)(k\eta)^3 E_d(k)/(\epsilon v^5)^{1/4}$ (dashed lines) for the DNS data at $R_\lambda \approx 340$ by Runs C512-1, C1024-2, C2048-4, and C4096-8.

The difference is only in their grid numbers, i.e., the resolution level. Conversely, we cannot observe the systematic dependence of the values of L_α and u_α on the resolution level, where $\alpha = s$ and d . Therefore, it implies that L_α and u_α are insensitive to the resolution level. (Note that the values of L_α and u_α can be influenced indirectly by the resolution level because our forcing depends on energy dissipation. Nevertheless, the influence was not visible in the values of L_α and u_α .) However, we can observe that the values of ϵ , ϵ_s , and ϵ_d in resolution level 1 are systematically smaller than their corresponding values in resolution level 2. This result indicates that the energy dissipation rates may be underestimated in the DNSs of the resolution level 1.

To acquire some idea of the resolution-level dependence of ϵ , ϵ_s , and ϵ_d , let us study the wave-number dependence of the spectra $k^2 E_s(k)$ and $k^2 E_d(k)$ at $R_\lambda \approx 330$ by Runs C512-1, C1024-2, C2048-4, and C4096-8. From Eqs. (14) and (15) we have

$$\begin{aligned} \epsilon &= 2\nu \int_0^\infty \{k^2 E_s(k) + (4/3)k^2 E_d(k)\} dk \\ &= 2\epsilon \int_0^\infty \{(k\eta)^2 E_s(k)/(\epsilon v^5)^{1/4} + (4/3)(k\eta)^2 E_d(k)/(\epsilon v^5)^{1/4}\} d(k\eta), \end{aligned}$$

where the last integral is a constant ($= 1/2$) by the definitions of ϵ and η . Noting that $\int k^2 E(k) dk \propto \int k^3 E(k) d(\ln k)$, we plot normalized values of $k^3 E_s(k)$ and $(4/3)k^3 E_d(k)$ as functions of the logarithm of $k\eta$ in Fig. 3. We can see that the main contribution to both solenoidal and dilatational energy dissipation for the case of $M_t \approx 0.3$ comes from a wave-number range at $k\eta \approx 0.3$. The plot shows that the shape of $k^3 E_s(k)$ for $k\eta < 1$ of Run C512-1 is mainly different from those of Runs C1024-2, C2048-4, and C4096-8. Furthermore, it reveals that the value of $k^3 E_d(k)$ at high $k\eta$ is not so small that it can be ignored. These result in the following: (i) to properly analyze the energy spectra for $k\eta < 1$, the value of $k_{\max}\eta$ ($\approx 3\eta/\Delta x$) should not be less than 2 in this DNS method of compressible turbulence, and (ii) to properly analyze the values of ϵ_d the resolution level should be higher than 2 for this case of $M_t \approx 0.3$.

B. Energy spectrum

The energy spectrum of turbulence is one of the most fundamental measures characterizing the statistics of turbulent flows. Compared with the energy spectrum of incompressible

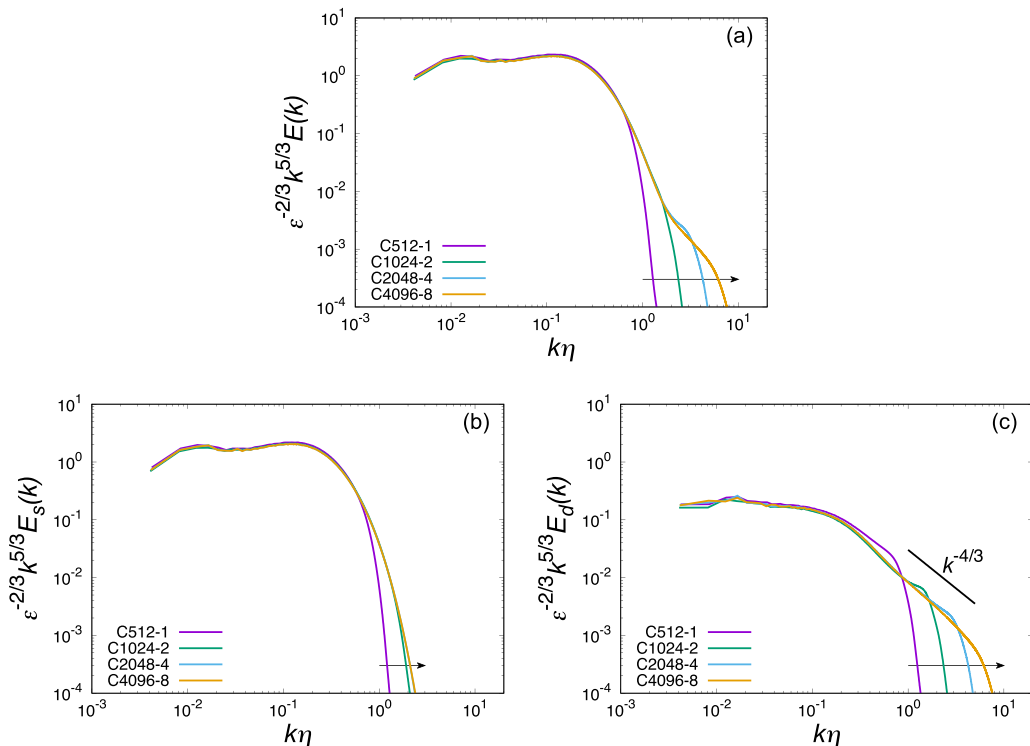


FIG. 4. (a) Compensated kinetic energy spectrum and its (b) solenoidal and (c) dilatational components. Arrows are directed toward the increasing resolution.

turbulence, the studies on the energy spectrum of compressible turbulence have been limited. DNS results by Donzis and Jagannathan [9] showed that the total energy spectra for $R_\lambda \approx 38\text{--}430$ and $M_t \approx 0.1, 0.3, 0.6$ are entirely consistent with incompressible results. However, they used solenoidal forcing, and the possible influence of the resolution level on the energy spectrum has not been discussed yet for the cases of nonsolenoidal forcing. Additionally, the energy spectrum in the dissipation range of compressible turbulence has not been extensively studied compared to incompressible turbulence (e.g., Refs. [69–75]). Therefore, it may be worthwhile to obtain some ideas on the potential influence of the resolution level on the energy spectrum of compressible turbulence.

Let us consider the possible influence of the resolution level (i.e., the choice of $k_{\max}\eta$). Figure 4(a) shows the compensated energy spectra $\epsilon^{-2/3}k^{5/3}E(k)$ obtained from DNSs with various resolutions in compressible isothermal turbulence at almost the same values of R_λ ($\approx 326\text{--}354$), $M_t \approx 0.3\text{--}0.33$, and $\delta \approx 0.39\text{--}0.4$. The spectra from different resolution levels in Fig. 4(a) have no remarkable difference for $k\eta \lesssim 0.6$. The spectra in the $k\eta \lesssim 0.6$ are consistent with those in Ref. [9]. However, as expected from Fig. 3, there are visible differences in the spectra for $k\eta \gtrsim 0.6$, i.e., the spectra expand toward the higher wave-number side as the resolution level increases.

To examine the resolution dependence of the energy spectrum in more detail, we investigate the solenoidal and dilatational components of the spectra in Figs. 4(b) and 4(c), respectively. Figure 4(b) shows that the solenoidal component of the energy spectrum does not depend on the resolution when $k_{\max}\eta \geq 4$. However, Fig. 4(c) demonstrates that, as the resolution level increases, the dilatational component of the energy spectrum spreads toward the high wave-number side suggesting a power law such as $E_d(k) \propto k^{-3}$. These results indicate that the solenoidal component of the energy spectrum almost converges when the smallest solenoidal eddies are resolved. In contrast,

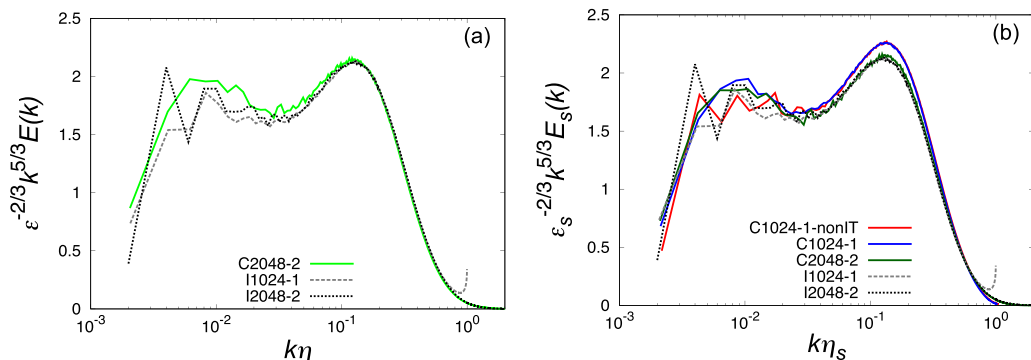


FIG. 5. (a) A plot of $\epsilon^{-2/3} k^{5/3} E(k)$ versus $k\eta$ for C2048-2, I1024-1, and I2048-2. (b) A plot of $\epsilon_s^{-2/3} k^{5/3} E_s(k)$ versus $k\eta_s$ for C1024-1-nonIT, C1024-1, C2048-2, I1024-1, and I2048-2.

the exceptionally high-resolution is required to accurately evaluate the dilatational component of the energy spectrum in compressible turbulence at $M_t \approx 0.3$. However, note that all normalized spectra, $E(k)$, $E_s(k)$, and $E_d(k)$, for $k\eta < 1$, are insensitive to the resolution levels provided that $k_{\max}\eta \gtrsim 2$. This study performed DNSs with no bulk viscosity, i.e., Stokes' hypothesis was applied. However, bulk viscosity can affect the dilatational component of the turbulent field. The effect of bulk viscosity on the kinetic energy spectrum is discussed in the Appendix.

Figure 5 compares the compensated energy spectrum of compressible turbulence and incompressible turbulence. To normalize the spectrum of compressible turbulence ϵ is used in Fig. 5(a), while ϵ_s is used instead in Fig. 5(b). Here, the dissipation rate ϵ_s , Kolmogorov length $\eta_s \equiv (\nu^3/\epsilon_s)^{1/4}$, and energy spectrum $E_s(k)$ in compressible isothermal turbulence are calculated using the solenoidal component of the velocity field. The compensated energy spectra in runs I1024-1 and I2048-2 are slightly different in the high wave-number range $k\eta \approx 1$ and the low wave-number range ($k\eta < 0.02$). The disparity of the spectra in these wave-number ranges, as stated in Ref. [2], is probably caused by the wave-number truncation at high k and the difference of the energy-containing eddies at the forcing scales. In contrast to the high and low wave-number ranges, the difference between the spectra in the other range ($0.02 < k\eta < 0.8$ in this case) for the two incompressible runs is very small. This result demonstrates that the spectrum of incompressible turbulence in the range is insensitive to the difference between $k_{\max}\eta \sim 1$ and $k_{\max}\eta \sim 2$, which agrees with the previous studies. Fig. 5 shows that the compensated spectrum of C2048-2 agrees well with those of I1024-1 and I2048-2 in the range ($0.02 < k\eta < 0.8$) when ϵ_s is used for the normalization instead of ϵ . Figure 5(b) shows that the compensated spectra in runs C1024-1 and C1024-1-nonIT agree well with each other in the range ($0.02 < k\eta < 0.8$). However, their agreement with C2048-2 (a compressible run with $k_{\max}\eta \sim 2$) in the range ($0.02 < k\eta < 0.8$) is not as good as in the case of incompressible turbulence. In general, the values of ϵ_s in resolution level 1 are smaller than those in level 2 (see Table II). Also, if the value of ϵ_s of C2048-2 is used, then the compensated energy spectrum of C1024-1 almost overlaps that of C2048-2 plotted in Fig. 5(b). Therefore, it can be explained that the difference in the spectra of C1024-1 and C2048-2 is mainly caused by the underestimation of the value of ϵ_s in C1024-1. In summary, the compensated spectrum obtained from the DNS of compressible isothermal turbulence with $k_{\max}\eta \gtrsim 2$ agrees well with that obtained from the DNS of incompressible turbulence when ϵ_s is used for the normalization instead of ϵ .

The Reynolds number dependence of the energy spectra obtained from compressible isothermal turbulence and incompressible turbulence are shown in Fig. 6. The result shows that the height of the energy spectrum at $k\eta \approx 0.13$ decreases with R_λ . The Reynolds number dependence of the spectral bump is also observed in the DNS results of incompressible turbulence [1,5]. According to Ishihara *et al.* [2], the wave-number range of the energy spectrum can be categorized into range

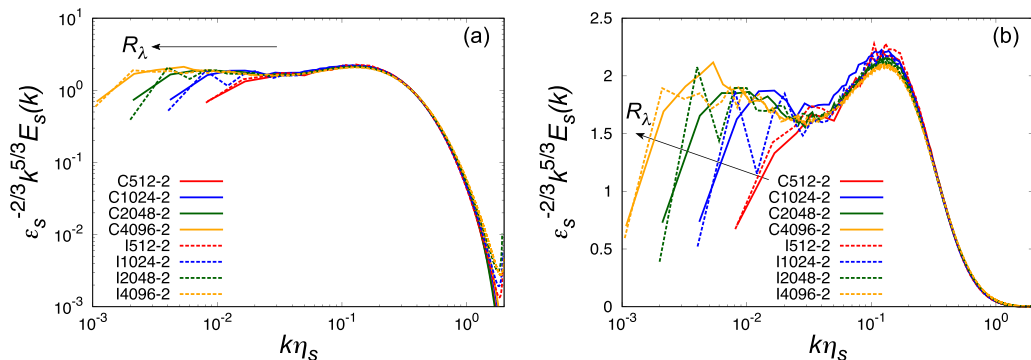


FIG. 6. Compensated energy spectra, $\epsilon_s^{-2/3} k^{5/3} E_s(k)$, as a function of $k\eta_s$ in (a) log-log scale and (b) linear-log scale. The arrows are directed toward increasing R_λ .

F ($k\eta \lesssim 5 \times 10^{-3}$), T ($5 \times 10^{-3} \lesssim k\eta \lesssim 2 \times 10^{-2}$), and B ($2 \times 10^{-2} \lesssim k\eta$). In Fig. 7(a), we show the solenoidal energy spectra for compressible isothermal turbulence with $R_\lambda = 520$ and the energy spectra for incompressible turbulence with $R_\lambda = 446$. It can be observed that the energy spectra almost overlap within the B range. Furthermore, in the results of DNSs with $R_\lambda \approx 800$ in Fig. 7(b), we find that the solenoidal energy spectrum for compressible isothermal turbulence and the energy spectrum for incompressible turbulence match even in the part of the T range. This result implies that the multiscale property of the solenoidal component of the velocity field in compressible isothermal turbulence agrees with that of the velocity field in incompressible turbulence. In incompressible turbulence, it is confirmed that the energy spectrum in the F range is significantly flatter than that in the T range [2]. Therefore, the F range is considered the candidate for the inertial subrange predicted by Kolmogorov [56] and Obukhov [76]. To confirm the existence of the F range in compressible turbulence, DNS of compressible turbulence with higher R_λ is required.

Figure 8 shows the compensated dilatational energy spectra obtained from the DNS series of the compressible isothermal turbulence with different Reynolds numbers of $R_\lambda = 183$ –840 at a turbulent Mach number of $M_t \approx 0.3$. We do not observe the scaling $E_d(k) \propto k^{-2}$ [i.e., $k^{5/3} E_d(k) \propto k^{-1/3}$] as observed in a hybrid numerical simulation of compressible turbulence at $M_t \approx 0.73$ and $R_\lambda \approx 210$ [12]. The highest Reynolds number possible for our compressible DNSs are significantly higher than that in the numerical simulations by Ref. [12]. However, the turbulent Mach number

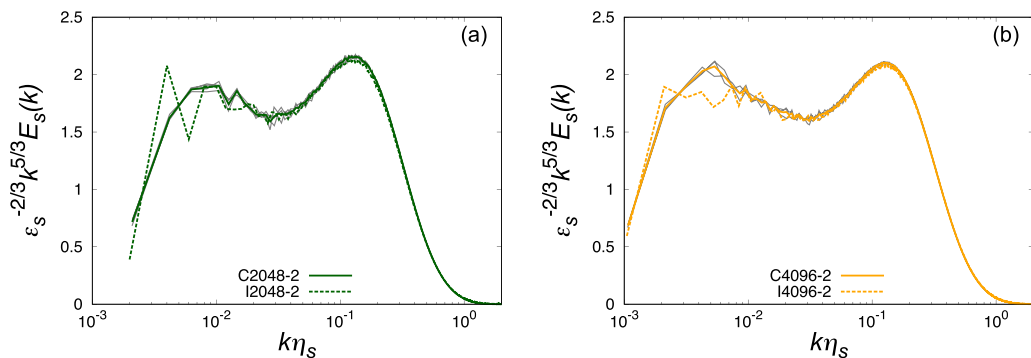


FIG. 7. Compensated energy spectra $\epsilon_s^{-2/3} k^{5/3} E_s(k)$ for (a) C2048-2 and I2048-2 and (b) C4096-2 and I4096-2. The gray lines in panels (a) and (b) show several snapshot data from (a) $t/T = 0.5$ –1.0 and (b) $t/T = 0.4$ –0.7, respectively. Here, $T = L/u$. Solid lines for C2048-2 in panel (a) and C4096-2 in panel (b) show the average over several snapshots represented in gray lines in panels (a) and (b), respectively.

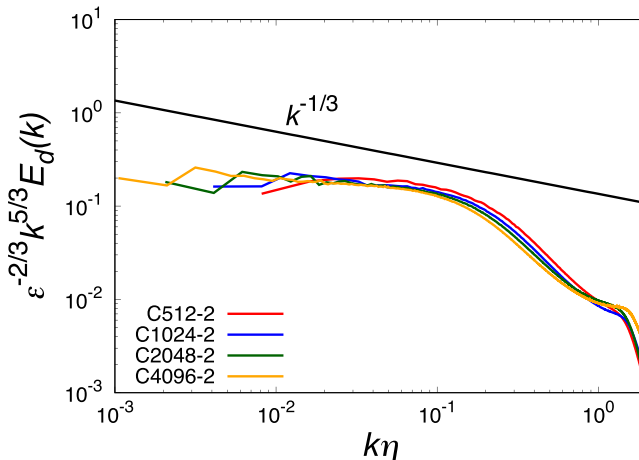


FIG. 8. Dilatational components of the compensated kinetic energy spectra.

in Ref. [12] is much higher than ours. Therefore, it is plausible to consider that the k^{-2} scaling of the compressive component of the kinetic energy spectrum in their simulation [12] comes from the shocks observed at $M_t \approx 0.73$ in Fig. 2(a) of Ref. [12]. We observed several jumps in density fluctuations that correspond to the shocklets in the DNSs of compressible isothermal turbulence; the result (figure omitted) is similar to Fig. 2(c) of Ref. [24]. A remarkable difference between the shocklets and the shocks can be visually observed by comparing these two figures.

Donzis and Jagannathan [9] compared the normalized dilatational energy spectrum for different Mach numbers $M_t \approx 0.1, 0.3,$ and 0.6 at the highest R_λ available for each case (i.e., 170, 430, and 170, respectively). See Fig. 10(b) in Ref. [9]. The figure shows that the value of each spectrum strongly depends on the values of M_t . For example, the value of the normalized dilatational energy spectrum in Fig. 8 is much higher than that of the case of $M_t \approx 0.3$ in Fig. 10(b) in Ref. [9]. The difference between our case and their case may come from the difference in the forcing scheme, i.e., a pure solenoidal forcing is used in Ref. [9], while solenoidal and dilatational components are forced in our cases.

C. PDFs of pressure and dilatation

Pressure fluctuations p' in compressible turbulence can be decomposed into solenoidal p^s and dilatational p^d pressures [23]. Here, the solenoidal component p^s is obtained by solving the Poisson equation

$$\nabla^2 p^s = \langle \rho \rangle \frac{\partial u_i^s}{\partial x_j} \frac{\partial u_j^s}{\partial x_i}, \quad (19)$$

and the dilatational component p^d is obtained by $p^d = p' - p^s$. A DNS study by Sakurai *et al.* [24] showed that the PDFs of p' in compressible nonisothermal turbulence depend on parameters such as M_t and δ , which characterize the compressible turbulence. It also shows that the PDFs of p^s in compressible turbulence are insensitive to such parameters and conform to the PDFs of p' in incompressible turbulence. Figure 9 shows that the pressure PDFs in compressible isothermal turbulence overlap relatively well, regardless of the Reynolds number. The values of M_t and δ for compressible isothermal turbulence in this study are almost the same (see Table I), so no remarkable difference can be observed in the pressure PDFs. The PDFs of p^s are negatively skewed in Fig. 9(b). They are qualitatively consistent with the PDFs of pressure fluctuations in incompressible turbulence [18–21]. The PDFs of p' and p^d are positively skewed in Figs. 9(a) and 9(c), respectively. All PDFs

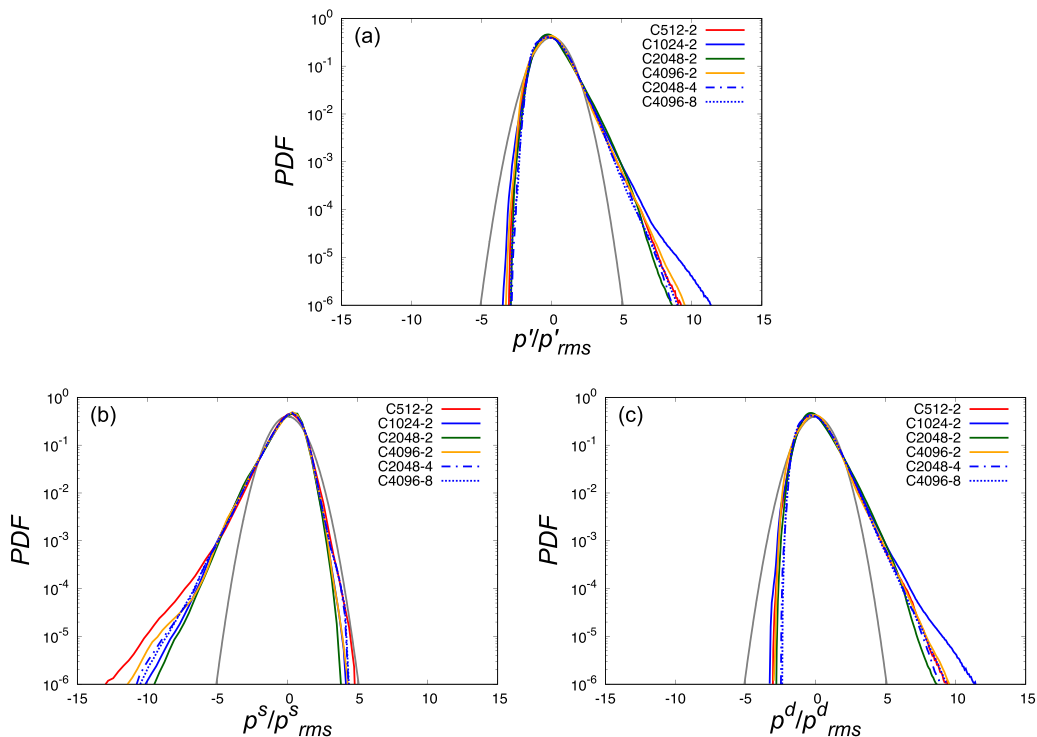


FIG. 9. PDFs of (a) pressure fluctuation p' , (b) solenoidal component p^s , and (c) dilatational component p^d . The values are normalized using the rms value. The gray lines represent a Gaussian distribution.

are consistent with the results obtained in compressible nonisothermal turbulence with $M_t \approx 0.3$ and $\epsilon_r \approx 0.1$ ($\delta \approx 0.4$) in Ref. [24]. This result indicates that the pressure field in the compressible turbulence is dominated by the dilatational component regardless of isothermal or nonisothermal. According to Ref. [10], the PDFs of p^d are close to Gaussian for negative fluctuations. However, the PDFs of p^d in Fig. 9(c) show platykurtic (light-tailed) compared to a Gaussian distribution for negative fluctuations. The difference in these results may be because of differences in forcing schemes; that is, a stochastic solenoidal forcing is used in Ref. [10], whereas a deterministic forcing in solenoidal and dilatational components is used in our study. The parameter study using the DNSs of compressible nonisothermal turbulence at $M_t = 0.1, 0.3$ and $\epsilon_r = 0, 0.01, 0.1$ [24] shows that the higher the values of M_t and ϵ_r , the higher the values of skewness of the PDFs of p^d , resulting in the relatively lighter tail of the negative parts.

The PDFs of p^s are compared in Fig. 10(a) to understand the difference between compressible isothermal and incompressible turbulence. All results exhibit negatively skewed fluctuations, indicating little differences in the solenoidal component of pressure fluctuations among different turbulent conditions. However, a close inspection of the PDFs indicates that p^s in compressible isothermal turbulence may be less intermittent than p^s in incompressible turbulence. In Fig. 10(b), we compare the PDFs of enstrophy in compressible isothermal turbulence with those in incompressible turbulence. Figure 10(b) shows that the tails are increasing functions of the Reynolds number and that the PDFs tails for incompressible turbulence are slightly heavier than those in compressible isothermal turbulence. The spikes of enstrophy are related to the significant negative values in pressure fluctuation (e.g., see Ref. [22]). Therefore, the less intermittent fluctuation of p^s in compressible isothermal turbulence is consistent with the less intermittent enstrophy fluctuations compared with incompressible turbulence.

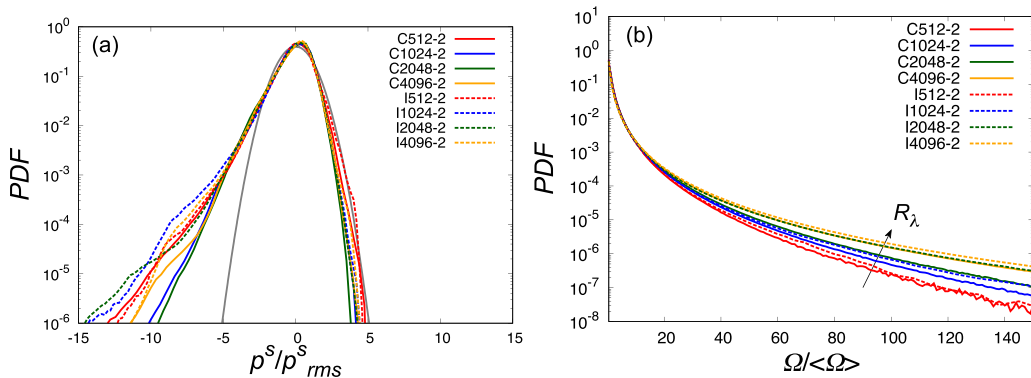


FIG. 10. (a) PDFs of solenoidal pressure fluctuations in compressible isothermal turbulence are compared with those of pressure fluctuations in incompressible turbulence. (b) The same as panel (a) but for the PDFs of entropy $\Omega = |\omega|^2/2$. The gray line in panel (a) represents a Gaussian distribution.

Finally, velocity divergence θ is examined as a statistic that characterizes compressible turbulence. In the present DNSs, all the compressible turbulent fields are obtained under almost the same conditions, i.e., $M_t \approx 0.3$ and $\delta \approx 0.4$. The PDFs of the normalized θ in Fig. 11(a) demonstrate that the larger the value of R_λ , the stronger the intermittency of the distribution of θ in compressible isothermal turbulence. The result is consistent with previous results of compressible nonisothermal turbulence [10,24,77]. As demonstrated in previous studies [36,37], we explored the resolution-level dependence of the intermittency in θ distribution and confirmed that the higher the resolution level, the stronger the intermittency (figure omitted). In Fig. 11(b), we compare the PDFs of θ/θ_{rms} in compressible isothermal turbulence with those in compressible nonisothermal turbulence using the data at the same resolution level (at $k_{max}\eta \sim 1.0$). The result implies that the isothermal assumption weakens the intermittency in velocity divergence in compressible turbulence. However, as revealed in the spectral analysis in Fig. 3, this suggestion should be examined using the DNSs with higher resolution levels (at $k_{max}\eta \gtrsim 2.0$).

D. Dilatational flow structures

We observed in Fig. 4(c) that the dilatational component of the energy spectrum in the DNS of the highest resolution level of $k_{max}\eta = 8$ exhibits a power law $E_d(k) \propto k^{-3}$ at a high k region. Wang

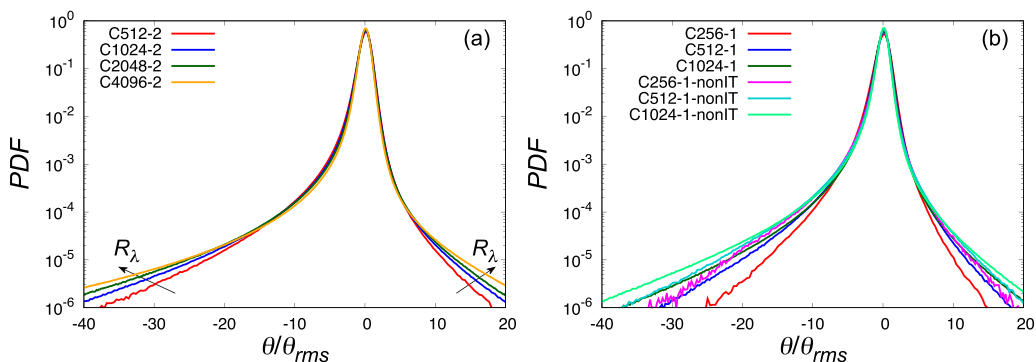


FIG. 11. (a) Reynolds number dependence of the PDFs of normalized velocity divergence in compressible isothermal turbulence at a resolution level ($k_{max}\eta \sim 2$). (b) PDFs of normalized velocity divergence in compressible isothermal turbulence at a resolution level ($k_{max}\eta \sim 1$) are compared with those obtained by the DNSs of compressible nonisothermal turbulence [24].

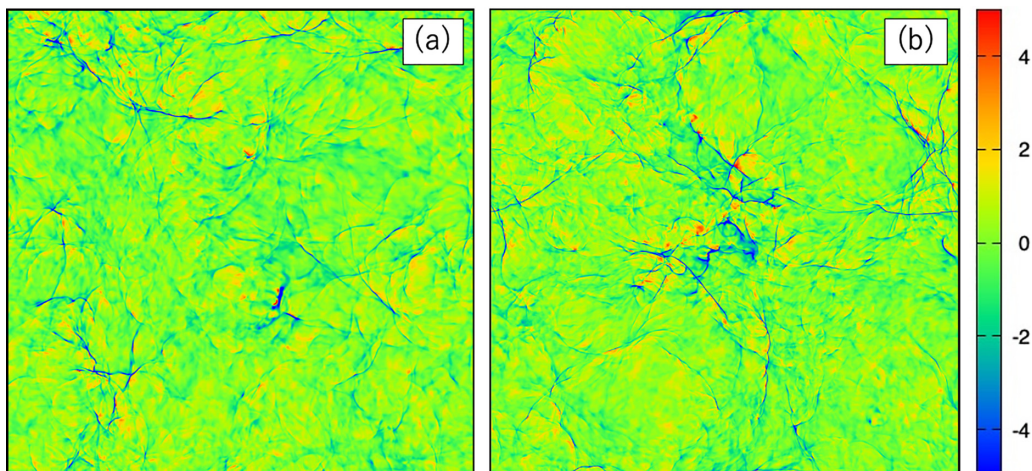


FIG. 12. Visualization of $\theta/\theta_{\text{rms}}$ on a slice of the field for (a) C1024-2 and (b) C4096-8.

et al. [8,12] observed a k^{-2} scaling in the compressive component of the kinetic energy spectrum in a hybrid numerical simulation of compressible turbulence at $M_t = 0.62$. They argued that the k^{-2} spectrum was given rise to as a consequence of the generation of large-scale shock waves. A k^{-3} scaling (steeper than the k^{-2} scaling) at a high k region can be explained by the existence of such a velocity profile expressed locally as

$$u(x) \propto \begin{cases} \sqrt{|x/\eta|} & (x < 0), \\ -\sqrt{x/\eta} & (x \geq 0), \end{cases}$$

where u is the x component of the velocity. This velocity profile has an infinite derivative at $x = 0$ and the resulting energy spectrum exhibits the k^{-3} scaling that unboundedly spreads toward high wave numbers. A velocity profile with a finite derivative at $x = 0$ can be obtained by smoothing. Therefore, analogous (smoothed) local velocity profiles may explain the occurrence of large negative absolute values of θ , i.e., shocklets, and the approximate k^{-3} scaling observed in Fig. 4(c).

Figure 12 shows contour plots of $\theta/\theta_{\text{rms}}$ obtained by C1024-2 and C4096-8. In both plots, we can observe several thin shocklets (thin regions with large negative absolute values of $\theta/\theta_{\text{rms}}$). The two plots are almost indistinguishable because the run parameters are the same except for the resolution

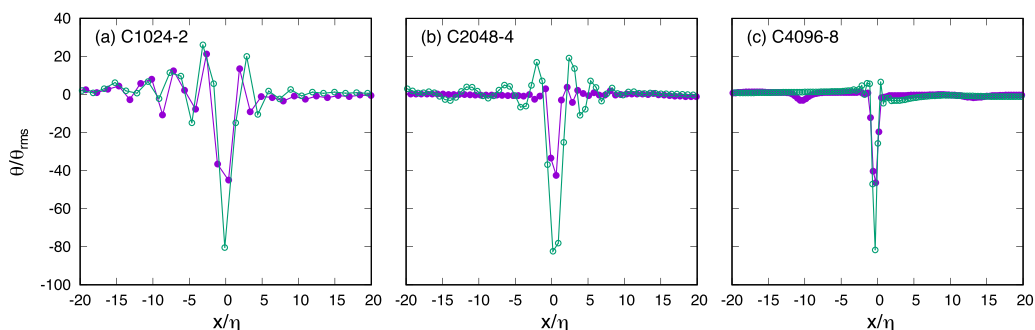


FIG. 13. Samples of the spatial variation of the values of $\theta/\theta_{\text{rms}}$ in the direction approximately normal to the shocklet around its large negative absolute values (40 and 80) in runs (a) C1024-2, (b) C2048-4, and (c) C4096-8.

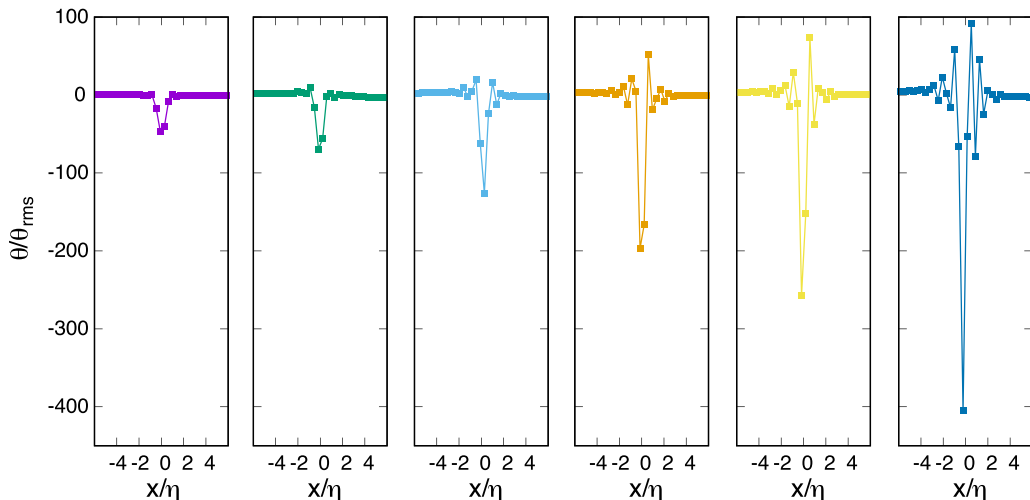


FIG. 14. Samples of the shocklet structure with various amplitudes of $\theta/\theta_{\text{rms}}$ in C4096-8.

level. However, a close inspection shows that shocklets observed in C4096-8 generally look thinner than those observed in C1024-2. To understand the resolution dependence, we compare in Fig. 13 the spatial variation of $\theta/\theta_{\text{rms}}$ near the relatively strong shocklets in runs C1024-2, C2048-4, and C4096-8. Figure 13 demonstrates the following: (i) Oscillation of $\theta/\theta_{\text{rms}}$ is observed on both sides of its large negative absolute value (local minimum). (ii) Amplitude of the oscillation becomes larger with the increase of the absolute value of the local minimum (from 40 to 80). (iii) The amplitude of the oscillation becomes smaller with the increase of the resolution level. (iv) The thickness of the shocklet (defined as the distance between the two local maxima nearest to the large negative absolute value) becomes smaller with the increase of the resolution level.

As shown in Fig. 11(a), the spatial volume in which $\theta/\theta_{\text{rms}} < -40$ is already very small. However, as suggested by the stretched exponential form of the negative side of the $(\theta/\theta_{\text{rms}})$'s PDF, much stronger shocklets (much smaller values of $\theta/\theta_{\text{rms}}$) are expected to exist in the whole computational domain. A thorough survey of the fields revealed that the minimum values for runs C1024-2, C2048-4, and C4096-8 are $\theta/\theta_{\text{rms}} = -110, -252,$ and -405 , respectively. This result indicates that the higher the resolution level the larger the absolute value of the minimum of $\theta/\theta_{\text{rms}}$ in the compressible turbulent flow field (at $M_t \approx 0.3$ and $\epsilon_r \approx 0.1$). Figure 14 illustrates that the larger the absolute values of the local minima of $\theta/\theta_{\text{rms}}$ in C4096-8 the larger the amplitude of the oscillations. As we have already observed in Fig. 13, for a fixed value of the local minimum of $\theta/\theta_{\text{rms}}$, the amplitude of the oscillations becomes smaller as the resolution level increases. Our result indicates that high spatial resolution simulations can capture thin and relatively strong shocklets which are not captured by low spatial resolution simulations. However, it is not known at present whether the k^{-3} scaling unboundedly spreads toward high wave numbers as the resolution level further increases. Also, it is not known how the oscillation accompanied by the minimum of $\theta/\theta_{\text{rms}}$ (the strongest shocklet) behaves as the resolution level further increases. To answer these questions, we need further large-scale computations.

IV. CONCLUSION

A series of the DNSs (maximum number of grid points $N^3 = 4096^3$) of compressible isothermal turbulence with the Mach number $M_t \approx 0.3$ and the ratio of dilatational to solenoidal rms velocities $\delta \approx 0.4$ was conducted, and the Reynolds number (R_λ) and resolution ($k_{\text{max}}\eta$) dependence of the statistics of compressible turbulence in the ranges of $R_\lambda = 183\text{--}853$ and $k_{\text{max}}\eta = 1\text{--}8$, respectively,

was investigated. Furthermore, the statistics of compressible isothermal turbulence were compared with those of incompressible turbulence and those of compressible nonisothermal turbulence. As a general conclusion, it was shown that the statistics computed using the solenoidal component of compressible turbulence agree well with those of incompressible turbulence.

As shown in Ref. [15], the classical incompressible scaling did not hold for the total energy dissipation field in compressible turbulence. Our DNSs confirmed that, as in the case of incompressible turbulence, the normalized solenoidal energy dissipation of compressible turbulence asymptotically takes a finite nonzero value (≈ 0.4) at high Reynolds numbers, i.e., in a range of the solenoidal Taylor Reynolds number $R_\lambda^s = 168\text{--}761$. However, the normalized dilatational energy dissipation values do not approach zero, as opposed to that expected in Ref. [15]. Instead, the values asymptotically approach a finite value at high Reynolds numbers (or may approach zero too slowly to observe in the range of the Reynolds numbers up to $R_\lambda^d = 453$). Spectral analysis of the energy dissipation reveals that the main contribution to solenoidal and dilatational energy dissipation for the case of $M_t \approx 0.3$ comes from the wave-number range at $k\eta \approx 0.3$. Furthermore, it was shown that the energy spectra obtained from the DNSs with a resolution level higher than 2 are convergent for $k\eta < 1$ in the case of $M_t \approx 0.3$.

The energy spectra for the compressible isothermal turbulence at $M_t \approx 0.3$ were found to expand to a higher wave-number range with increasing the resolution levels of the DNS. The solenoidal components of the energy spectra almost converge for $k_{\max}\eta \gtrsim 4$. Conversely, the dilatational components of the energy spectra at high wave numbers do not converge even for $k_{\max}\eta > 4$ and spread toward the high wave-number side suggesting a k^{-3} scaling. Note, however, that the changes in the spectrum become relatively smaller as the resolution levels increase. These results indicate that very high-resolution simulations are required to accurately resolve the behavior of the dilatational component at small scales in compressible turbulence (at $M_t \approx 0.3$).

As for the energy spectra of compressible isothermal turbulence for $k\eta < 1$, both the solenoidal and dilatational components are not very sensitive to the resolution levels provided that $k_{\max}\eta \gtrsim 2$. We confirmed that the solenoidal component of the energy spectrum normalized using solenoidal energy dissipation is consistent with the compensated energy spectrum of incompressible turbulence in the bump (B) range and in the tilted (T) range. To observe the flat (F) range in the energy spectrum of compressible turbulence, we need much larger-scale DNSs of compressible turbulence. The dilatational component of the energy spectra exhibits neither the k^{-2} scaling nor the $k^{-5/3}$ scaling in the inertial range. Comparison with the previous studies [9,12] shows that the amplitude of the normalized dilatational component of energy spectra strongly depends on the turbulent Mach number and the forcing scheme, as suggested by Refs. [14,24].

The properties of the pressure fluctuations in compressible isothermal turbulence are consistent with the previous study based on the DNSs of compressible nonisothermal turbulence in Ref. [24]. The PDFs of the solenoidal component p^s of pressure fluctuations are consistent with those of incompressible turbulence. However, a precise comparison of the PDFs of p^s and enstrophy in compressible isothermal turbulence with those in incompressible turbulence shows that the solenoidal pressure and enstrophy fluctuations in compressible isothermal turbulence are consistently less intermittent than those in incompressible turbulence. Furthermore, we compared the PDFs of the normalized velocity divergence $\theta/\theta_{\text{rms}}$ in compressible isothermal turbulence with those in compressible nonisothermal turbulence using the data at a similar resolution level (at $k_{\max}\eta \sim 1$). The result indicates that the isothermal assumption weakens the intermittency in velocity divergence in compressible turbulence. However, we should check this result using the DNSs with higher resolution levels at $k_{\max}\eta \gtrsim 2$.

ACKNOWLEDGMENTS

This work used computational resources of the Supercomputer Fugaku provided by the RIKEN Center for Computational Science, the FX1000 system at the Information Technology Center, Nagoya University, and Ito Subsystem A at the Research Institute for Information Technology,

TABLE III. Simulation parameters and turbulence characteristics.

Run	N^3	$k_{\max}\eta$	$10^3\Delta t$	μ_b/μ	R_λ	M_t	δ	ϵ_r	$10^2\epsilon$	$10^3\eta$
C512-1-0	512^3	1.03	0.5	0	354	0.30	0.39	0.101	6.97	4.21
C1024-2-0	1024^3	1.99	0.5	0	326	0.33	0.39	0.098	8.02	4.07
C2048-4-0	2048^3	4.05	0.1	0	337	0.33	0.40	0.120	7.48	4.14
C512-1-1	512^3	1.00	0.5	1	334	0.33	0.36	0.109	7.73	4.10
C1024-2-1	1024^3	1.96	0.5	1	316	0.33	0.36	0.108	8.44	4.02
C2048-4-1	2048^3	3.91	0.1	1	315	0.33	0.37	0.116	8.57	4.00
C512-1-30	512^3	0.98	0.5	30	318	0.33	0.32	0.107	8.47	4.01
C1024-2-30	1024^3	1.93	0.5	30	304	0.33	0.30	0.096	8.96	3.96
C2048-4-30	2048^3	3.87	0.1	30	304	0.33	0.30	0.098	8.94	3.96

Kyushu University, through the HPCI System Research Project (Project No. hp230143). This research was supported by Grant-in-Aid for JSPS Research Fellow (Grant No. JP20J13073) and JSPS KAKENHI (Grant No. JP20H01948).

APPENDIX: EFFECT OF BULK VISCOSITY ON THE KINETIC ENERGY SPECTRUM

The kinetic energy spectra in compressible isothermal turbulence with no bulk viscosity were investigated in the main text. The result showed that the dilatational component of the spectrum in high wave-number regions depends on the resolution levels of the DNSs. In this Appendix, we study

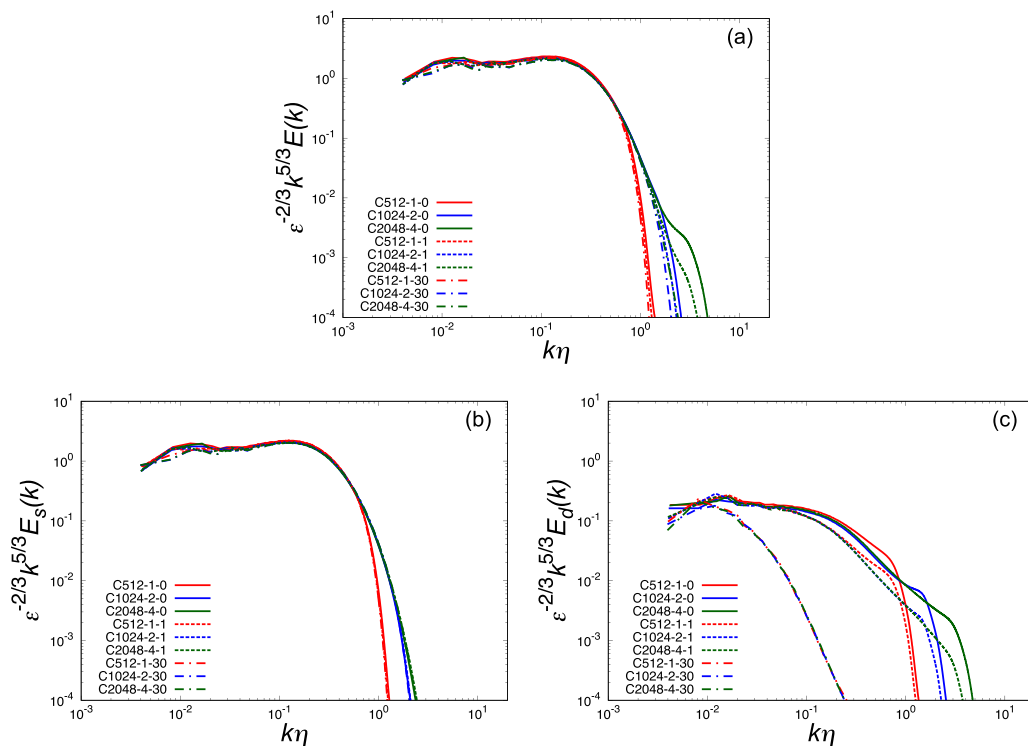


FIG. 15. Effect of bulk viscosity on (a) compensated kinetic energy spectrum and its (b) solenoidal and (c) dilatational components.

the effect of bulk viscosity on the kinetic energy spectra. In the DNSs of compressible isothermal turbulence with bulk viscosity, the viscous stress tensor is replaced by

$$\tau_{ij} = \mu \left(\frac{\partial u_i}{\partial x_j} + \frac{\partial u_j}{\partial x_i} - \frac{2}{3} \theta \delta_{ij} \right) + \mu_b \theta \delta_{ij}, \quad (\text{A1})$$

where μ_b is the bulk viscosity [78,79]. Here, the ratio of the bulk viscosity μ_b to the shear viscosity μ is set as $\mu_b/\mu = 0, 1, 30$. The values $\mu_b/\mu = 0, 1$, and 30 correspond to the cases of no bulk viscosity, air, and H_2 , respectively [78]. The DNS parameters and turbulence characteristics are summarized in Table III. The last number in run names in Table III represents the values of μ_b/μ . The compressible dissipation per unit mass is defined as $\epsilon_d = ((4/3)\mu(\theta^2) + \mu_b(\theta^2))/(\rho)$ [78].

Figure 15(a) shows that the compensated kinetic energy spectrum in the high wave-number range depends on the value of bulk viscosity. The effect of bulk viscosity is more pronounced, especially in the case of high spatial resolution. As observed in high spatial resolution results shown in Figs. 15(a) and 15(c), the bulk viscosity suppresses the dilatational component of the energy spectrum at a high k region and makes the scaling of the spectrum at the high k region steeper. However, it can be observed from Fig. 15(b) that bulk viscosity does not affect the solenoidal component of the energy spectrum. Thus, the suppression of the energy spectrum is solely because of the change of the dilatational component affected by the bulk viscosity.

-
- [1] T. Ishihara, T. Gotoh, and Y. Kaneda, Study of high-Reynolds number isotropic turbulence by direct numerical simulation, *Annu. Rev. Fluid Mech.* **41**, 165 (2009).
 - [2] T. Ishihara, K. Morishita, M. Yokokawa, A. Uno, and Y. Kaneda, Energy spectrum in high-resolution direct numerical simulations of turbulence, *Phys. Rev. Fluids* **1**, 082403(R) (2016).
 - [3] M. Kiya and H. Ishii, Vortex interaction and Kolmogorov spectrum, *Fluid Dyn. Res.* **8**, 73 (1991).
 - [4] Y. Tsuji, Intermittency effect on energy spectrum in high-Reynolds number turbulence, *Phys. Fluids* **16**, L43 (2004).
 - [5] D. A. Donzis and K. R. Sreenivasan, The bottleneck effect and the Kolmogorov constant in isotropic turbulence, *J. Fluid Mech.* **657**, 171 (2010).
 - [6] S. Lee, S. K. Lele, and P. Moin, Eddy shocklets in decaying compressible turbulence, *Phys. Fluids A* **3**, 657 (1991).
 - [7] R. Samtaney, D. I. Pullin, and B. Kosovic, Direct numerical simulation of decaying compressible turbulence and shocklet statistics, *Phys. Fluids* **13**, 1415 (2001).
 - [8] J. Wang, Y. Yang, Y. Shi, Z. Xiao, X. T. He, and S. Chen, Cascade of Kinetic Energy in Three-Dimensional Compressible Turbulence, *Phys. Rev. Lett.* **110**, 214505 (2013).
 - [9] D. A. Donzis and S. Jagannathan, Fluctuations of thermodynamic variables in stationary compressible turbulence, *J. Fluid Mech.* **733**, 221 (2013).
 - [10] S. Jagannathan and D. A. Donzis, Reynolds and Mach number scaling in solenoidally-forced compressible turbulence using high-resolution direct numerical simulations, *J. Fluid Mech.* **789**, 669 (2016).
 - [11] S. Kida and S. A. Orszag, Energy and spectral dynamics in forced compressible turbulence, *J. Sci. Comput.* **5**, 85 (1990).
 - [12] J. Wang, Y. Yang, Y. Shi, Z. Xiao, X. T. He, and S. Chen, Statistics and structures of pressure and density in compressible isotropic turbulence, *J. Turbulence* **14**, 21 (2013).
 - [13] J. Wang, T. Gotoh, and T. Watanabe, Spectra and statistics in compressible isotropic turbulence, *Phys. Rev. Fluids* **2**, 013403 (2017).
 - [14] D. A. Donzis and J. P. John, Universality and scaling in homogeneous compressible turbulence, *Phys. Rev. Fluids* **5**, 084609 (2020).
 - [15] J. P. John, D. A. Donzis, and K. R. Sreenivasan, Does dissipative anomaly hold for compressible turbulence? *J. Fluid Mech.* **920**, A20 (2021).

- [16] M. E. Brachet, Direct simulation of three-dimensional turbulence in the Taylor-Green vortex, *Fluid Dyn. Res.* **8**, 1 (1991).
- [17] S. Fauve, C. Laroche, and B. Castaing, Pressure fluctuations in swirling turbulent flows, *J. Phys. II France* **3**, 271 (1993).
- [18] A. Pumir, A numerical study of pressure fluctuations in three-dimensional, incompressible, homogeneous, isotropic turbulence, *Phys. Fluids* **6**, 2071 (1994).
- [19] P. Vedula and P. K. Yeung, Similarity scaling of acceleration and pressure statistics in numerical simulations of isotropic turbulence, *Phys. Fluids* **11**, 1208 (1999).
- [20] N. Cao, S. Chen, and G. D. Doolen, Statistics and structures of pressure in isotropic turbulence, *Phys. Fluids* **11**, 2235 (1999).
- [21] Y. Tsuji and T. Ishihara, Similarity scaling of pressure fluctuation in turbulence, *Phys. Rev. E* **68**, 026309 (2003).
- [22] S. Douady, Y. Couder, and M. E. Brachet, Direct Observation of the Intermittency of Intense Vorticity Filaments in Turbulence, *Phys. Rev. Lett.* **67**, 983 (1991).
- [23] P. Sagaut and C. Cambon, *Homogeneous Turbulence Dynamics* (Cambridge University Press, Cambridge, UK, 2008).
- [24] Y. Sakurai, T. Ishihara, H. Furuya, M. Umemura, and K. Shiraishi, Effects of the compressibility of turbulence on the dust coagulation process in protoplanetary disks, *Astrophys. J.* **911**, 140 (2021).
- [25] Y. Yamazaki, T. Ishihara, and Y. Kaneda, Effects of wave-number truncation on high-resolution direct numerical simulation of turbulence, *J. Phys. Soc. Jpn.* **71**, 777 (2002).
- [26] J. Schumacher, K. R. Sreenivasan, and P. K. Yeung, Very fine structures in scalar mixing, *J. Fluid Mech.* **531**, 113 (2005).
- [27] P. K. Yeung, S. B. Pope, A. G. Lamorgese, and D. A. Donzis, Acceleration and dissipation statistics of numerically simulated isotropic turbulence, *Phys. Fluids* **18**, 065103 (2006).
- [28] T. Watanabe and T. Gotoh, Inertial-range intermittency and accuracy of direct numerical simulation for turbulence and passive scalar turbulence, *J. Fluid Mech.* **590**, 117 (2007).
- [29] T. Ishihara, Y. Kaneda, M. Yokokawa, K. Itakura, and A. Uno, Small-scale statistics in high-resolution direct numerical simulation of turbulence: Reynolds number dependence of one-point velocity gradient statistics, *J. Fluid Mech.* **592**, 335 (2007).
- [30] D. A. Donzis, P. K. Yeung, and K. R. Sreenivasan, Dissipation and enstrophy in isotropic turbulence: Resolution effects and scaling in direct numerical simulations, *Phys. Fluids* **20**, 045108 (2008).
- [31] D. A. Donzis and P. K. Yeung, Resolution effects and scaling in numerical simulations of passive scalar mixing in turbulence, *Physica D* **239**, 1278 (2010).
- [32] P. K. Yeung, K. R. Sreenivasan, and S. B. Pope, Effects of finite spatial and temporal resolution in direct numerical simulations of incompressible isotropic turbulence, *Phys. Rev. Fluids* **3**, 064603 (2018).
- [33] P. K. Yeung and K. Ravikumar, Advancing understanding of turbulence through extreme-scale computation: Intermittency and simulations at large problem sizes, *Phys. Rev. Fluids* **5**, 110517 (2020).
- [34] J. Jiménez, A. A. Wray, P. G. Saffman, and R. S. Rogallo, The structure of intense vorticity in isotropic turbulence, *J. Fluid Mech.* **255**, 65 (1993).
- [35] T. Watanabe, K. Tanaka, and K. Nagata, Solenoidal linear forcing for compressible, statistically steady, homogeneous isotropic turbulence with reduced turbulent Mach number oscillation, *Phys. Fluids* **33**, 095108 (2021).
- [36] J. Wang, Y. Shi, L.-P. Wang, Z. Xiao, X. T. He, and S. Chen, Effect of shocklets on the velocity gradients in highly compressible isotropic turbulence, *Phys. Fluids* **23**, 125103 (2011).
- [37] J. Wang, Y. Shi, L.-P. Wang, Z. Xiao, X. T. He, and S. Chen, Effect of compressibility on the small scale structures in isotropic turbulence, *J. Fluid Mech.* **713**, 588 (2012).
- [38] J. Poggie, N. J. Bisek, and R. Gosse, Resolution effects in compressible, turbulent boundary layer simulations, *Comput. Fluids* **120**, 57 (2015).
- [39] L. Liu, J. Wang, Y. Shi, S. Chen, and X. T. He, A hybrid numerical simulation of supersonic isotropic turbulence, *Commun. Comput. Phys.* **25**, 189 (2019).

- [40] P. Padoan, B. J. T. Jones and Å. P. Nordlund, Supersonic turbulence in the interstellar medium: Stellar extinction determinations as probes of the structure and dynamics of dark clouds, *Astrophys. J.* **474**, 730 (1997).
- [41] A. G. Kritsuk, M. L. Norman, P. Padoan, and R. Wagner, The statistics of supersonic isothermal turbulence, *Astrophys. J.* **665**, 416 (2007).
- [42] C. Federrath, R. S. Klessen, and W. Schmidt, The density probability distribution in compressible isothermal turbulence: Solenoidal versus compressive forcing, *Astrophys. J.* **688**, L79 (2008).
- [43] D. J. Price, C. Federrath, and C. M. Brunt, The density variance-mach number relation in supersonic, isothermal turbulence, *Astrophys. J.* **727**, L21 (2011).
- [44] C. A. Nolan, C. Federrath, and R. S. Sutherland, The density variance-Mach number relation in isothermal and non-isothermal adiabatic turbulence, *Mon. Notices R. Astron. Soc.* **451**, 1380 (2015).
- [45] L. Pan and P. Padoan, Turbulence-induced relative velocity of dust particles. I. Identical particles, *Astrophys. J.* **776**, 12 (2013).
- [46] R. F. Hopkins and H. Lee, The fundamentally different dynamics of dust and gas in molecular clouds, *Mon. Not. R. Astron. Soc.* **456**, 4174 (2016).
- [47] T. S. Tricco, D. J. Price, and G. Laibe, Is the dust-to-gas ratio constant in molecular clouds? *Mon. Notices R. Astron. Soc.* **471**, L52 (2017).
- [48] L. Mattsson, A. Bhatnagar, F. A. Gent and B. Villarroel, Clustering and dynamic decoupling of dust grains in turbulent molecular clouds, *Mon. Notices R. Astron. Soc.* **483**, 5623 (2019).
- [49] M. R. Petersen and D. Livescu, Forcing for statistically stationary compressible isotropic turbulence, *Phys. Fluids* **22**, 116101 (2010).
- [50] S. Sarkar, G. Erlebacher, M. Y. Hussaini, and H. O. Kreiss, The analysis and modelling of dilatational terms in compressible turbulence, *J. Fluid Mech.* **227**, 473 (1991).
- [51] Y. Kaneda, T. Ishihara, K. Morishita, M. Yokokawa, and A. Uno, Statistics of local Reynolds number in box turbulence: Ratio of inertial to viscous forces, *J. Fluid Mech.* **929**, A1 (2021).
- [52] S. K. Lele, Compact finite difference schemes with spectral-like resolution, *J. Comput. Phys.* **103**, 16 (1992).
- [53] N. Mattor, T. J. Williams, and D. Hewett, Algorithm for solving tridiagonal matrix problems in parallel, *Parallel Comput.* **21**, 1769 (1995).
- [54] S. Gottlieb and C. W. Shu, Total variation diminishing Runge-Kutta schemes, *Math. Comput.* **67**, 73 (1998).
- [55] D. V. Gaitonde and M. R. Visbal, High-order schemes for Navier-Stokes equations: Algorithms and implementation into FDL3DI, Tech. Report No. AFRL-VA-WP-TR-1998-3060, Air Force research Laboratory, Wright-Patterson AFB, 1998.
- [56] A. N. Kolmogorov, The local structure of turbulence in incompressible viscous fluid for very large Reynolds numbers, *Dokl. Acad. Nauk SSSR* **30**, 299 (1941).
- [57] K. R. Sreenivasan, On the scaling of the turbulence energy-dissipation rate, *Phys. Fluids* **27**, 1048 (1984).
- [58] B. R. Pearson, P. A. Krogstad, and W. van de Water, Measurements of the turbulent energy dissipation rate, *Phys. Fluids* **14**, 1288 (2002).
- [59] P. C. Valente and J. C. Vassilicos, The decay of turbulence generated by a class of multiscale grids, *J. Fluid Mech.* **687**, 300 (2011).
- [60] L. Wang, S. Chen, J. G. Brasseur, and J. C. Wyngaard, Examination of hypotheses in the Kolmogorov refined turbulence theory through high-resolution simulations. Part 1. Velocity field, *J. Fluid Mech.* **309**, 113 (1996).
- [61] K. R. Sreenivasan, An update on the energy dissipation rate in isotropic turbulence, *Phys. Fluids* **10**, 528 (1998).
- [62] Y. Kaneda, T. Ishihara, M. Yokokawa, K. Itakura, and A. Uno, Energy dissipation rate and energy spectrum in high resolution direct numerical simulations of turbulence in a periodic box, *Phys. Fluids* **15**, L21 (2003).
- [63] D. A. Donzis, K. R. Sreenivasan, and P. K. Yeung, Scalar dissipation rate and dissipative anomaly in isotropic turbulence, *J. Fluid Mech.* **532**, 199 (2005).

- [64] W. J. T. Bos, L. Shao, and J. P. Bertoglio, Spectral imbalance and the normalized dissipation rate of turbulence, *Phys. Fluids* **19**, 045101 (2007).
- [65] W. D. McComb, A. Berera, M. Salewski, and S. Yoffe, Taylor's (1935) dissipation surrogate reinterpreted, *Phys. Fluids* **22**, 061704 (2010).
- [66] C. Doering and C. Foias, Energy dissipation in body-forced turbulence, *J. Fluid Mech.* **467**, 289 (2002).
- [67] J. C. Vassilicos, Dissipation in turbulent flows, *Annu. Rev. Fluid Mech.* **47**, 95 (2015).
- [68] D. A. Donzis, K. R. Sreenivasan, and P. K. Yeung, The Batchelor spectrum for mixing of passive scalars in isotropic turbulence, *Flow, Turbul. Combust.* **85**, 549 (2010).
- [69] S. Chen, G. Doolen, J. R. Herring, R. H. Kraichnan, S. A. Orszag, and Z. S. She, Far-Dissipation Range of Turbulence, *Phys. Rev. Lett.* **70**, 3051 (1993).
- [70] D. O. Martinez, S. Chen, G. D. Doolen, R. H. Kraichnan, L. P. Wang, and Y. Zhou, Energy spectrum in the dissipation range of fluid turbulence, *J. Plasma Phys.* **57**, 195 (1997).
- [71] T. Ishihara, Y. Kaneda, M. Yokokawa, K. Itakura, and A. Uno, Energy spectrum in the near dissipation range of high resolution direct numerical simulation of turbulence, *J. Phys. Soc. Jpn.* **74**, 1464 (2005).
- [72] J. Schumacher, Sub-Kolmogorov-scale fluctuations in fluid turbulence, *Europhys. Lett.* **80**, 54001 (2007).
- [73] S. Khurshid, D. A. Donzis, and K. R. Sreenivasan, Energy spectrum in the dissipation range, *Phys. Rev. Fluids* **3**, 082601(R) (2018).
- [74] D. Buaria and K. R. Sreenivasan, Dissipation range of the energy spectrum in high Reynolds number turbulence, *Phys. Rev. Fluids* **5**, 092601(R) (2020).
- [75] A. Gorbunova, G. Balarac, M. Bourgoïn, L. Canet, N. Mordant, and V. Rossetto, Analysis of the dissipative range of the energy spectrum in grid turbulence and in direct numerical simulations, *Phys. Rev. Fluids* **5**, 044604 (2020).
- [76] A. M. Obukhov, On the distribution of energy in the spectrum of turbulent flow, *Dokl. Akad. Nauk SSSR* **32**, 22 (1941).
- [77] J. Wang, T. Gotoh, and T. Watanabe, Shocklet statistics in compressible isotropic turbulence, *Phys. Rev. Fluids* **2**, 023401 (2017).
- [78] S. Pan and E. Johnsen, The role of bulk viscosity on the decay of compressible homogeneous isotropic turbulence, *J. Fluid Mech.* **833**, 717 (2017).
- [79] S. Chen, X. Wang, J. Wang, M. Wan, S. Li, and H. Chen, Effects of bulk viscosity on compressible homogeneous turbulence, *Phys. Fluids* **31**, 085115 (2019).